

Available online at www.sciencedirect.com**ScienceDirect**

Physics Procedia 69 (2015) 104 – 108

Physics

Procedia

10 World Conference on Neutron Radiography 5-10 October 2014

The CG-1D neutron imaging beamline at the Oak Ridge National Laboratory High Flux Isotope Reactor

Lou Santodonato^{a,*}, Hassina Bilheux^a, Barton Bailey^a, Jean Bilheux^a, Phong Nguyen^a,
Anton Tremsin^b, Doug Selby^a, and Lakeisha Walker^a

^a Oak Ridge National Laboratory, Neutron Sciences Directorate, Oak Ridge, TN 37831, USA^b University of California, Space Sciences Laboratory, Berkeley, CA 94720 USA

Abstract

The Oak Ridge National Laboratory Neutron Sciences Directorate has installed a neutron imaging beamline at the High Flux Isotope Reactor (HFIR) cold guide hall. CG-1D is one of the three instruments that make up the CG1 instrument suite. The beamline optics and detector have recently been upgraded to meet the needs of the neutron imaging community (better “smoothing” of guide system artifacts, higher flux or spatial resolution). These upgrades comprise a new diffuser/aperture system, two new detectors, a He-filled flight tube and silicon (Si) windows. Shielding inside the flight tube, beam scrapers and a beam stop ensure that biological dose is less than 50 $\mu\text{Sv/hr}$ outside of the radiation boundary.

A set of diffusers and apertures (pinhole geometry) has been installed at the exit of the guide system to allow motorized L/D variation. Samples sit on a translation/rotation stage for alignment and tomography purposes. Detectors for the CG-1D beamline are (1) an ANDOR DW936 charge coupled device (CCD) camera with a field of view of approximately 7 cm x 7 cm and ~ 80 microns spatial resolution and 1 frame per second time resolution, (2) a new Micro-Channel Plate (MCP) detector with a 2.8 cm x 2.8 cm field of view and 55 microns spatial resolution, and 5 μs timing capability. $^6\text{LiF/ZnS}$ scintillators of thickness varying from 50 to 200 microns are being used at this facility. An overview of the beamline upgrade and preliminary data is presented here.

© 2015 The Authors. Published by Elsevier B.V. This is an open access article under the CC BY-NC-ND license (<http://creativecommons.org/licenses/by-nc-nd/4.0/>).

Selection and peer-review under responsibility of Paul Scherrer Institut

* Corresponding author. Tel.: +1-865-719-0656; fax: +1-865-241-6770.

E-mail address: santodonatol@ornl.gov

Notice: This manuscript has been authored by UT-Battelle, LLC, under Contract No. DE-AC05-00OR22725 with the U.S. Department of Energy. The United States Government retains and the publisher, by accepting the article for publication, acknowledges that the United States Government retains a non-exclusive, paid-up, irrevocable, world-wide license to publish or reproduce the published form of this manuscript, or allow others to do so, for United States Government purposes.

Keywords: neutron radiography; cold neutrons; beamline optics; aperture; diffuser; CCD; MCP.

1. Introduction

Neutron imaging is a non-invasive non-destructive technique that is complementary to other imaging techniques such as X-ray, Magnetic Resonance Imaging (MRI) or gamma imaging. Due to the interaction properties of neutrons with matter, some light nuclei such as *H* greatly scatter neutrons whereas some heavier elements such as *Cu* or *Pb* are not strong scatterers or absorbers of neutrons and can therefore be easily penetrated. Neutron imaging encompasses a broad range of applications (Anderson et al. 2009).

Neutron radiography measures the attenuation of a neutron beam caused by absorption and scattering within a sample, using a two-dimensional position-sensitive detector that measures the transmitted neutron flux. The beam attenuation caused by a homogeneous uniformly thick sample composed of a single isotope is given by

$$I(\lambda) = I_0(\lambda)e^{-\mu(\lambda)\Delta x} \quad (1)$$

where I_0 and I are, respectively, the incident and transmitted beam intensities, μ is the attenuation coefficient, λ is the neutron wavelength, and Δx is the thickness of the sample. The attenuation coefficient μ is given by

$$\mu(\lambda) = \sigma_t(\lambda) \frac{\rho N_A}{M} \quad (2)$$

where $\sigma_t(\lambda)$ is the material's total cross section for neutrons, ρ is its density, N_A is Avogadro's number, and M is the molar mass. Attenuation coefficients (i.e. neutron attenuation) are wavelength dependent as described in Eq. 2. Straightforward extension of these basic formulas underpins the radiography of heterogeneous and irregularly shaped objects.

Recent developments have demonstrated the importance of performing wavelength-dependent neutron imaging which provides unique contrast mechanisms and access to, for example, crystalline plane and texture information, otherwise unavailable in white beam measurements. Thus, ORNL is planning to build a state-of-the-art neutron imaging facility at the Spallation Neutron Source named VENUS (H. Bilheux et al., these proceedings). In white beam measurements, only the average value of $\sigma_t(\lambda)$ is probed rather than its value at different wavelengths. Wavelength-discrete $\sigma_t(\lambda)$ values can be achieved at neutron pulsed sources by TOF technique (Tremisn et al. 2012) or by the use of a monochromatic beam at reactor sources (Kardjilov et al. 2009), thus enhancing contrast in the object under investigation. Although VENUS will eventually take the lead in wavelength-dependent neutron imaging at ORNL, the existing CG-1D instrument (Crow et al. 2010) will continue to be a neutron imaging workhorse. The recent CG-1D upgrades have opened up new capabilities, such as time-resolved studies, and the user demand is steadily increasing.

2. Instrument layout

The CG-1D instrument (Fig. 1) is located at the end of a cold neutron guide, viewing a liquid hydrogen moderator. A motorized aperture/diffuser system is installed at the guide exit, within a steel enclosure. The flight path from the aperture to detector is 6.59 m. A helium-filled flight tube, with Si windows and motorized boron-nitride exit slits, is installed between the steel enclosure and the sample position. Interchangeable sample tables and rotation stages are available to accommodate a variety of sample sizes and special sample environments. The detector assembly is installed on a linear stage, which allows routine exchange between the CCD and MCP devices. The instrument boundary is defined by a fence, which allows high visibility and monitoring of the experimental set-up, and controls access with an interlocked sliding gate.

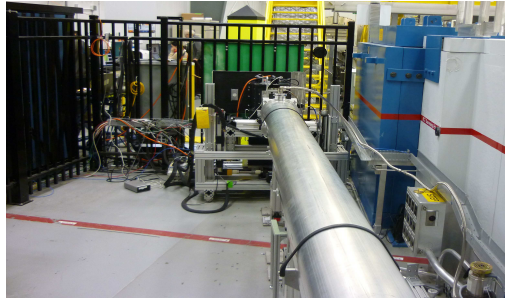


Fig. 1. Photo looking downstream along the flight tube.

3. Beam optics upgrades

The beamline optics have recently been upgraded with a new motorized aperture/diffuser system allowing the changes of L/D from 400 to 2000, where L is the distance from the aperture to the detector (6.59 m), and D is the aperture diameter. The aperture is defined by a tapered Cadmium (Cd) knife-edge backed by a 6 mm thick boron nitride (BN) layer. Five different aperture diameters are available (3.3, 4.1, 8.2, 11, and 16 mm). The diffusers may be independently selected, in order to reduce the sharp vertical and horizontal intensity fluctuations caused by the neutron guide (Fig. 2a). Two types of diffusers were installed, 50 nm Al_2O_3 nanoparticles and Carbon (C) powder, of thicknesses varying from 0.1 to 10 mm. By changing the thickness and type of diffuser, the beam artefact removal at the cost of lower neutron flux and increased beam divergence can be achieved. For most experiments the 4mm Al_2O_3 diffuser is used, because it has acceptable beam transmission (90%) and beam artefacts can be removed efficiently during normalization of the radiographs.

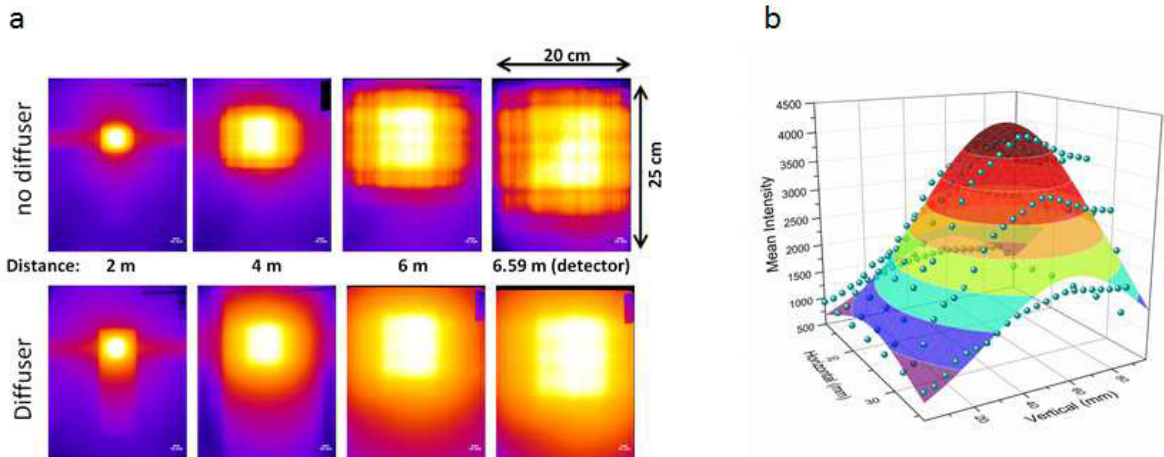


Fig. 2. (a) A series of neutron image plate measurements at various distances from the aperture indicate a 2.7-degree beam divergence with the 4 mm Al_2O_3 diffuser in place, using the 16 mm aperture. The smoothing and increased beam size effects of the nanoparticle diffuser can be seen by comparing the top and bottom radiographs. (b) The aperture position was optimized with respect to the neutron guide, in order to find the maximum integrated neutron flux on the detector.

During commissioning of the new optics, image plates were installed along the neutron flight path to measure radiographs of the beam profile (Fig. 2a). A 2.7-degree beam divergence was measured. The plate measurements were taken with and without the 4mm Al_2O_3 diffuser and the 16 mm aperture in place. Its effect can be seen by examining Fig. 2a. In a separate beam optics test, the position of the aperture/diffuser assembly was varied with

respect to the neutron guide in steps of the radius of the 8.2 and 11 mm apertures, respectively. Open beam images were taken at each position to determine the brightness as a function of aperture position. Each point on Fig. 2b represents the mean grayscale value of an open beam measurement for a given aperture position. After data analysis, it was found that the aperture position that corresponds to the maximum flux on sample is 2 cm below the vertical center of the guide system.

4. Detector upgrades

Motorized translation between detectors is available at the CG-1D beamline. One detector is a CCD-based system (Koerner et. al 2000), consisting of a camera focused on a neutron-sensitive 50 μm thick $^6\text{LiF/ZnS}$ scintillator. It has a field of view of approximately 7 cm x 7 cm, ~ 80 microns spatial resolution, and 1 frame per second time resolution (Kang et al. 2013). The detector is housed within a light-tight box, which may be translated transverse to the neutron beam direction. A new MCP detector (Tremisn et al. 2009) has been mounted on the side of the box, allowing motorized translation between the two detectors (Fig. 3). The MCP has a 2.8 x 2.8 cm field of view, and 55 μm spatial resolution (equal to its pixel size) in the normal imaging mode. Radiographs with 15 μm spatial resolution are possible using the centroiding mode (Tremisn et al. 2012). The MCP has 1 μs timing capability in the thermal and cold neutron range, which has been used for dynamic studies of processes such as fuel injection. It is also heavily used for tomography on small samples.

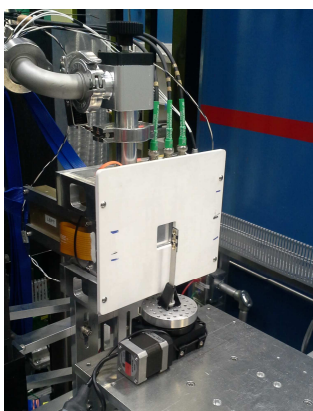


Fig. 3. Photograph of the MCP detector. The white front plate is made of boron nitride, for neutron shielding, with a square cutout in the center for the 2.8 cm x 2.8 cm detector area. High voltage (-2.5 kV) and signal cables are connected at the top, as well as the high-vacuum pump port. Below the detector is a rotation stage and sample holder used for tomography scans.

5. Conclusion and outlook

The upgraded CG-1D neutron imaging beamline at the HFIR is heavily subscribed for a wide variety of experiments. Future upgrades will allow upstream sample and detector placement to take advantage of higher flux for dynamic studies. The imaging team is currently working on expanding sample environment capabilities to respond to the scientific community demand. With the planned addition of the VENUS instrument at the SNS, imaging is a major part of the neutron sciences program at ORNL.

Acknowledgements

This research was supported by the Laboratory Directed Research and Development (LDRD) Program of ORNL, and was conducted at ORNL's High Flux Isotope Reactor, sponsored by the Scientific User Facilities Division, Office of Basic Energy Sciences, US Department of Energy. The authors are thankful from contributions from Dr. Lowell Crow, the HFIR support groups, the HFIR Machine Shop, and Mrs. Lisa Fagan.

References

- Anderson, I. S., McGreevy, R., Bilheux, H. S., Neutron imaging and applications: a reference for the imaging community, Springer, 2009.
- Crow, L., Robertson, L., Bilheux, H., Fleenor, M., Iverson, E., Tong, X., Stoica, D., Lee W.T., The CG1 instrument development test station at the high flux isotope reactor, Nuclear Instruments and Methods in Physics Research Section A: Accelerators, Spectrometers, Detectors and Associated Equipment, 634 (2011) S71-S74.
- Kang, M., Bilheux, H.Z., Voisin, S., Cheng, C.L., Perfect, E., Horita, J., Warren, J.M. 2013. Water calibration measurements for neutron radiography: Application to water content quantification in porous media. Nuclear Instruments and Methods in Physics Research A 708, 24-31.
- Kardjilov, N., Hilger, A., Manke, I., Strobl, M., Dawson, M., Banhart, J., New trends in neutron imaging, Nuclear Instruments and Methods in Physics Research A 605 (2009) 13-15.
- Koerner, S., Lehmann, E., Vontobel, P., Design and optimization of a CCD-neutron radiography detector, Nuclear Instruments and Methods in Physics Research Section A: Accelerators, Spectrometers, Detectors and Associated Equipment, 454 (2000) 158-164.
- Tremsin, A.S., McPhate, J.B., Vallerger, J.V., Siegmund, O.H.W., Hull, J.S., Feller, W.B., Lehmann, E., Detection efficiency, spatial and timing resolution of thermal and cold neutron counting MCP detectors, Nuclear Instruments and Methods in Physics Research Section A: Accelerators, Spectrometers, Detectors and Associated Equipment, 604 (2009) 140-143.
- Tremsin, A. S., McPhate, J. B., Vallerger, J. V., Siegmund, O. H. W., Feller, W. B., Lehmann, E., Kaestner, A., Boillat, P., Panzner, T., Filges, U., M., Neutron radiography with sub-15 μm resolution through event centroiding, Nuclear Instruments and Methods in Physics Research A 688 (2012) 32-40.
- Tremsin, A. S., McPhate, J. B., Steuwer, A., Kockelmann, W., Paradowska, A. M., Kelleher, J. F., Vallerger, J. V., Siegmund, O. H. W., Feller, W. B., High resolution strain mapping through time-of-flight neutron transmission diffraction with a micro channel plate neutron counting detector, Strain 48 (2012) 296-305.